

Micro-crack detection of nonlinear Lamb wave propagation in three-dimensional plates with mixed-frequency excitation

Wei-Guang Zhu(祝伟光)[1], Yi-Feng Li(李义丰)[1,2], Li-Qiang Guan(关立强)[1], Xi-Li Wan(万夕里)[1], Hui-Yang Yu(余辉洋)[1], Xiao-Zhou Liu(刘晓宙)[3]

Citation: Chin. Phys. B . 2020, 29(1): 014302 . **doi:** 10.1088/1674-1056/ab5931
Journal homepage: http://cpb.iphy.ac.cn; http://iopscience.iop.org/cpb

What follows is a list of articles you may be interested in

Simulation of acoustic fields emitted by ultrasonic phased array in austenitic steel weld

Zhong-Cun Guo(郭忠存)[1,2], Shou-Guo Yan(阎守国)[1], Bi-Xing Zhang(张碧星)[1,2]

Chin. Phys. B . 2019, 28(11): 114302 . **doi:** 10.1088/1674-1056/ab4d41

Lamb waves topological imaging combining with Green's function retrieval theory to detect near filed defects in isotropic plates

Hui Zhang(张辉), Hai-Yan Zhang(张海燕), Meng-Yun Xu(徐梦云), Guo-Peng Fan(范国鹏), Wen-Fa Zhu(朱文发), Xiao-Dong Chai(柴晓冬)

Chin. Phys. B . 2019, 28(7): 074301 . **doi:** 10.1088/1674-1056/28/7/074301

Seismoelectric wave propagation modeling in a borehole in water-saturated porous medium having an electrochemical interface

Hao-Ran Ding(丁浩然), Jin-Xia Liu(刘金霞), Zhi-Wen Cui(崔志文), Tribikram Kundu

Chin. Phys. B . 2017, 26(12): 124301 . **doi:** 10.1088/1674-1056/26/12/124301

Three-dimensional parabolic equation model for seismo-acoustic propagation:Theoretical development and preliminary numerical implementation

Jun Tang(唐骏), Sheng-Chun Piao(朴胜春), Hai-Gang Zhang(张海刚)

Chin. Phys. B . 2017, 26(11): 114301 . **doi:** 10.1088/1674-1056/26/11/114301

Rayleigh reciprocity relations: Applications

Ju Lin(林巨), Xiao-Lei Li(李小雷), Ning Wang(王宁)

Chin. Phys. B . 2016, 25(12): 124303 . **doi:** 10.1088/1674-1056/25/12/124303

Micro-crack detection of nonlinear Lamb wave propagation in three-dimensional plates with mixed-frequency excitation*

Wei-Guang Zhu(祝伟光)[1], Yi-Feng Li(李义丰)[1,2,†], Li-Qiang Guan(关立强)[1], Xi-Li Wan(万夕里)[1], Hui-Yang Yu(余辉洋)[1], and Xiao-Zhou Liu(刘晓宙)[3]

[1] *College of Computer Science and Technology, Nanjing Tech University, Nanjing* 211800, *China*
[2] *Key Laboratory of Modern Acoustics, Ministry of Education, Nanjing University, Nanjing* 210093, *China*
[3] *Key Laboratory of Modern Acoustics, Ministry of Education, Institute of Acoustics and School of Physics, Nanjing University, Nanjing* 210093, *China*

(Received 20 October 2019; revised manuscript received 17 November 2019; accepted manuscript online 20 November 2019)

We propose a nonlinear ultrasonic technique by using the mixed-frequency signals excited Lamb waves to conduct micro-crack detection in thin plate structures. Simulation models of three-dimensional (3D) aluminum plates and composite laminates are established by ABAQUS software, where the aluminum plate contains buried crack and composite laminates comprises cohesive element whose thickness is zero to simulate delamination damage. The interactions between the S_0 mode Lamb wave and the buried micro-cracks of various dimensions are simulated by using the finite element method. Fourier frequency spectrum analysis is applied to the received time domain signal and fundamental frequency amplitudes, and sum and difference frequencies are extracted and simulated. Simulation results indicate that nonlinear Lamb waves have different sensitivities to various crack sizes. There is a positive correlation among crack length, height, and sum and difference frequency amplitudes for an aluminum plate, with both amplitudes decreasing as crack thickness increased, *i.e.*, nonlinear effect weakens as the micro-crack becomes thicker. The amplitudes of sum and difference frequency are positively correlated with the length and width of the zero-thickness cohesive element in the composite laminates. Furthermore, amplitude ratio change is investigated and it can be used as an effective tool to detect inner defects in thin 3D plates.

Keywords: nonlinear Lamb wave, mixed-frequency, micro-cracks, amplitude ratio

PACS: 43.20.+g, 43.35.+d **DOI:** 10.1088/1674-1056/ab5931

1. Introduction

Thin plate structures are widely used in engineering fields, such as shipbuilding, railway vehicles, and aerospace. However, barely visible fatigue damage and cracks are often caused by a variety of processing factors, including external impact, chemical corrosion, thermal fatigue, *etc*. Therefore, the detection of early micro-cracks is essential to avoid engineering factor and structure failures with consequential potentially disastrous accidents. Nondestructive testing (NDT)[1] techniques have been previously verified to meet the requirements for real-time and reliability, and, combined with recently developed measurement and calculation methods, they become irreplaceable techniques for structural health monitoring (SHM)[2] applications. The SHM systems can monitor structural changes instantly, and provide damage diagnosis to effectively judge the structure health and outline a reasonable maintenance plan.[3] Ultrasonic Lamb wave techniques have been extensively used for thin plate NDT, since they can transfer energy long distance and detect internal defects by interrogating the whole thickness of the structure.[4,5]

Conventional ultrasonic Lamb wave techniques are universally based on linear theory and usually dependent on measuring several specific parameters, including acoustic velocity, and transmission and reflection coefficients, to confirm material elastic properties or evaluate the damage. However, the measured data are sensitive to open cracks, macroscopic damage, or through-holes, thus causing significant transmission barriers, whereas they are much less sensitive to evenly distributed micro-cracks or material degradation prior to forming visible damage.[6,7] Consequently, ultrasonic NDT methods based on linear theory are not suitable for detecting the buried micro-cracks.

Nonlinear ultrasonic techniques can beak through accuracy and sensitivity limitations.[8,9] The main distinction between linear and nonlinear ultrasound technique lies in the fact that the defect features for the latter are often associated with another acoustic signal whose frequency differs from the excitation signals. Ultrasonic wave nonlinearity encompasses nonlinear phenomena such as wave distortion, harmonic generation, and sideband formation when the ultrasonic wave propagates in materials. At present, nonlinear ultrasonic techniques have been widely studied in the areas of nonlinear ultrasonic resonance spectroscopy,[10] high order harmonics,[11] and subharmonic and mixing responses.[12] Nonlinear ultrasonic technique applications have been investigated as effective methods to overcome linear technique deficiencies.[13,14]

*Project supported by the National Natural Science Foundation of China (Grant Nos. 61571222, 61602235, and 11474160) and the Six Talent Peaks Project of Jiangsu Province, China.

†Corresponding author. E-mail: lyffz4637@163.com

© 2020 Chinese Physical Society and IOP Publishing Ltd

Nonlinear Lamb wave detection techniques have received increasingly attention due to their long propagation distance and high detection efficiency in thin plate structures.[15,16] Many general researches and simulation studies are based on nonlinear Lamb wave testing for non-destructive evaluation (NDE). Several studies have considered defect instances and nonlinear attribute influences for single material plate and composite laminates, most of which focus on higher harmonics (mainly second harmonic) generated from micro-cracks. Wang *et al.*[17] investigated fatigue damage identification in carbon fibre reinforced steel plates; Zhao *et al.*[18] analyzed nonlinear Lamb wave generation mechanism with random micro-crack distributions. Sotoudeh *et al.*[19] installed specific sensors to obtain the nonlinear Lamb wave response signals experimentally, acquiring delamination damage approximate dimension and location by using the damage imaging method. Yang *et al.*[20] investigated the crack opening and the influence of incident wave angle on Lamb wave second harmonic generation. Li *et al.*[21] used nonlinear Lamb wave to detect material degradation during thermal cycling. Most of nonlinear Lamb wave studies considered single-frequency excitation. However, the harmonic generation is practically difficult due to its non-determinacy, *i.e.*, it is hard to judge whether the measured nonlinearity is caused by defect or experimental devices.[22]

Nonlinear Lamb wave mixing is an effective method to break through these recognized limitations, based on the influence of material nonlinear attributes between the two intersecting ultrasound waves.[22] Nonlinear Lamb wave mixing relies on the interaction characteristics between two incident waves of different frequencies in the structure, thus achieving the considerable detection of inner defect. If the structure is successive, no new frequency components will be generated when the two waves meet. On the contrary, if the structure is non-successive, interactions will occur in associated regions when the two waves meet in the nonlinear region, resulting in the coupling the two waves. New frequency components will be generated in the frequency domain, including sum and difference frequencies. The wave mixing technique has unique advantages compared with the second-harmonics-generating traditional nonlinear ultrasonic techniques. Different detection regions can be scanned over by adjusting the excitation location of wave mixing.[23] Second, wave modes, frequencies, and propagation directions have great and relatively flexible selectivity to avoid redundant harmonics caused by some experimental device in a testing system.[24] Nonlinear Lamb wave mixing detection hasreceived increasingly attention due to its great potential to detect micro-cracks and damage, which has gradually been used in NDT. Lee *et al.*[25] studied the feasibility of Lamb wave mixing nonlinear technique for detecting the defects in thin plates.

The main purpose of this paper is to investigate damage detection effects for nonlinear Lamb waves by using mixing excitation in propagation through three-dimensional (3D) thin plate (aluminum plate and composite laminates) structures. We first introduce the basic nonlinear Lamb wave frequency mixing theory, and then establish a 3D finite element model based on mixing excitation by using ABAQUS software[23] to generate Lamb wave S mode signal. Nonlinear relationships between S mode signals and different dimensional cracks are discussed. Amplitude ratio variation is also analyzed and clearly demonstrates the nonlinear correlation between Lamb wave and crack dimensions in an intuitive manner.

2. Basic theory of nonlinear Lamb wave

2.1. Excitation and mode selection of Lamb wave

Ultrasonic Lamb waves are stress waves generated by acoustic guided waves propagating in a homogeneous and isotropic thin plate structure, where the plate thicknesshas the same order of magnitude as the excitation signal wavelength.[22] Lamb waves are formed in thin plates by successive reflections, transmissions, and mode transformations due to interactions with structural boundaries. According to whether particle vibrations are symmetrical with respect to the center plane of the plate, Lamb waves can be divided into symmetric and anti-symmetric modes.[26,27] Symmetric modes include S_0, S_1, S_2, ..., S_n, and anti-symmetric modes include A_0, A_1, A_2, ..., A_n. Dispersive and multimodal Lamb wave characteristics can be described by the Raleigh–Lamb relationship[28]

$$\frac{\tan qh/2}{\tan ph/2} = -\left[\frac{4pqk^2}{(k^2-q^2)^2}\right]^{\pm 1}, \tag{1}$$

where k is the wave number in the direction of propagation; h is the plate thickness; exponent ± 1 expresses symmetric and anti-symmetric mode, respectively; w is the angular frequency;[29]

$$p^2 = \left(\frac{w}{c_l}\right)^2 - k^2, q^2 = \left(\frac{w}{c_t}\right)^2 - k^2, \tag{2}$$

with c_l and c_t denoting the longitudinal and transverse wave velocity inside the plate, respectively.

As shown in Eq. (1), Lamb wave propagation has dispersive and multi-mode aspects. Dispersion is the most important feature, *i.e.*, propagation velocity depends on not only material properties, but also the incident wave frequency. Figure 1 shows phase and group velocity (C_p and C_g, respectively) dispersion curves for a Lamb wave propagating in an aluminum plate.

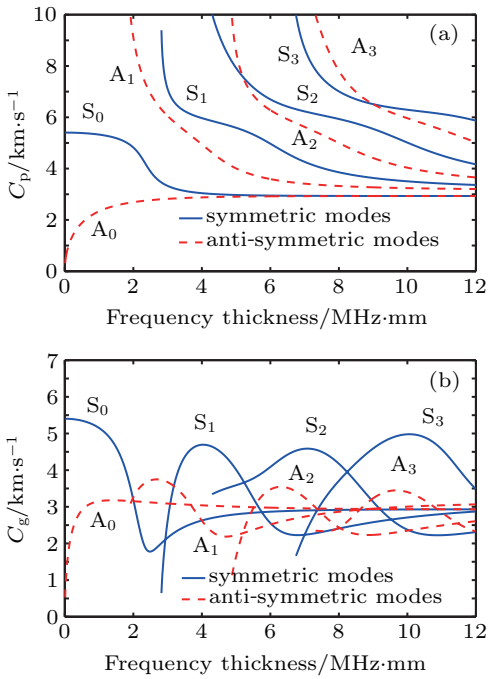


Fig. 1. Lamb wave dispersion in aluminum plate, showing (a) C_p and (b) C_g *versus* frequency.

Wave interaction propagating in multiple layered composites generally depends on the frequency, geometry, constituent properties, and propagation direction. Theoretical curves for composite laminates can be calculated from the Vallen Dispersion program, version R2017.0504.2, from Vallen–Systeme GmbH.[30]

Consequently, appropriate lower frequencies should be chosen to display only two fundamental modes (S_0 and A_0), thus making them analyzed conveniently and simply. We select the original symmetric mode (S_0 mode) as the desirable method for nonlinear Lame wave mixing excitation used in NDT. The reason is that the S_0 mode is virtually non-dispersive, significantly reducing signal complexity; stress is relatively uniform through the plate thickness, hence microcrack sensitivity is not reliant on the thickness of damaged region; and this is the fastest mode, ensuring that it will be the first wave packet to reach the receiving destination, hence simply distinguishing superfluous signals.[22,31] Thus, an appropriate excitation manner should be selected to produce the single S_0 mode.

2.2. Lamb wave nonlinear mixing effect

Nonlinear mixing effect is associated with material nonlinear elastic behavior, *i.e.*, the relationship between stress, σ, and strain, ε, is nonlinear, which can be described by the nonlinear Hooke law[32]

$$\sigma = E_0\varepsilon(1+\beta\varepsilon+\cdots), \tag{3}$$

where E_0 is the Young's modulus and β is the second order nonlinear elastic coefficient, called the acoustic nonlinearity parameter in this paper.

Due to the existence of nonlinear sources, such as crack damage in the structure, system input and output can be simplified into

$$f(t) = \alpha u(t) + \beta u^2(t) + h(t), \tag{4}$$

where $u(t)$ represents the incident signal; $f(t)$ is the system response; α and β are constants representing the first- and second-order nonlinear coefficients, respectively; and $h(t)$ is an undefined function to represent noise, which is ignored in the following discussion.

Suppose that an incoming signal consists of two sinusoidal signals with different frequencies,

$$u(t) = A_1\cos(2\pi f_1 t + k_1 x) + A_2\cos(2\pi f_2 t + k_2 x), \tag{5}$$

where x is the displacement; A_1, A_2 and f_1, f_2 represent the two sinusoidal signal amplitudes and frequencies, respectively; and k_1 and k_2 are the signal wave numbers.[22] Then, regardless of the reflection of the S_0 mode signal, the corresponding solution can be expressed as

$$\begin{aligned} f(t) = {} & \beta\frac{A_1^2+A_2^2}{2} + \alpha A_1\cos(2\pi f_1 t + k_1 x) \\ & + \alpha A_2\cos(2\pi f_2 t + k_2 x) \\ & + \frac{\beta A_1^2}{2}\cos[2\pi(2f_1)t + 2k_1 x] \\ & + \frac{\beta A_2^2}{2}\cos[2\pi(2f_2)t + 2k_2 x] \\ & + \beta A_1 A_2\cos[2\pi(f_2+f_1)t + (k_2+k_1)x] \\ & + \beta A_1 A_2\cos[2\pi(f_2-f_1)t + (k_2-k_1)x], \end{aligned} \tag{6}$$

and we can make Eq. (6) Fourier transformed into

$$\begin{aligned} F(f) = {} & \frac{\alpha A_1}{2}\delta(f-f_1)\mathrm{e}^{\mathrm{j}k_1 x} + \frac{\alpha A_2}{2}\delta(f-f_2)\mathrm{e}^{\mathrm{j}k_2 x} \\ & + \frac{\beta A_1^2}{4}\delta(f-2f_1)\mathrm{e}^{\mathrm{j}2k_1 x} + \frac{\beta A_2^2}{4}\delta(f-2f_2)\mathrm{e}^{\mathrm{j}2k_2 x} \\ & + \frac{\beta A_1 A_2}{2}\delta[f-(f_2+f_1)]\mathrm{e}^{\mathrm{j}(k_1+k_2)x} \\ & + \frac{\beta A_1 A_2}{2}\delta[f-(f_2-f_1)]\mathrm{e}^{\mathrm{j}(k_2-k_1)x}, \end{aligned} \tag{7}$$

which describes nonlinear system effect for mixed-frequency excitation.

Thus, interaction between the two sinusoidal signal components appears due to nonlinear stress-strain relationship, thus generating two new frequency components: sum frequency and difference frequency.[22]

The acoustic nonlinear coefficient, β, can be simplified into

$$\beta = \frac{|A_1 \pm A_2|}{A_1 A_2}, \tag{8}$$

where A_1 and A_2 represent the fundamental frequency signal amplitudes, respectively.[12,22,33]

In this paper we analyze the time domain signals received from 3D simulation model in the frequency domain using fast Fourier transform (FFT). A_1 and A_2 can be relatively easily measured and calculated, and β is also called the amplitude ratio, which can be used as a damage evaluation parameter for buried micro-cracks in thin plates.

3. The 3D finite element simulation

3.1. The 3D model

We established 3D numerical simulations and performed explicit dynamic analyses by using ABAQUS Dynamic/Explicit. The software was used to simulate nonlinear Lamb waves propagating in both aluminum plate and composite laminates.

3.1.1. The 3D model of aluminum plate

Table 1 presents the finite element model dimensions and material parameters for the aluminum plate, and Fig. 2 shows the 3D model dimensions and plate damage. The excitation signal was applied to the left plate surface in the form of transient force (Fig. 2), thus generating the expected S_0 mode Lamb wave signal. The mixed excitation signal was composed of two Hanning-windowed 5-cycle tone burst signals with 100-kHz and 350-kHz center frequencies in the aluminum plate. Figure 3 shows the excitation signal and the corresponding frequency domain spectrum.

Table 1. Model dimensions and aluminum plate material parameters.

Dimensions (length × width× height)/mm^3	Density ρ/(kg/m^3)	Elasticity modulus E/GPa	Poisson's ratio λ
1000×40× 2	2700	69	0.33

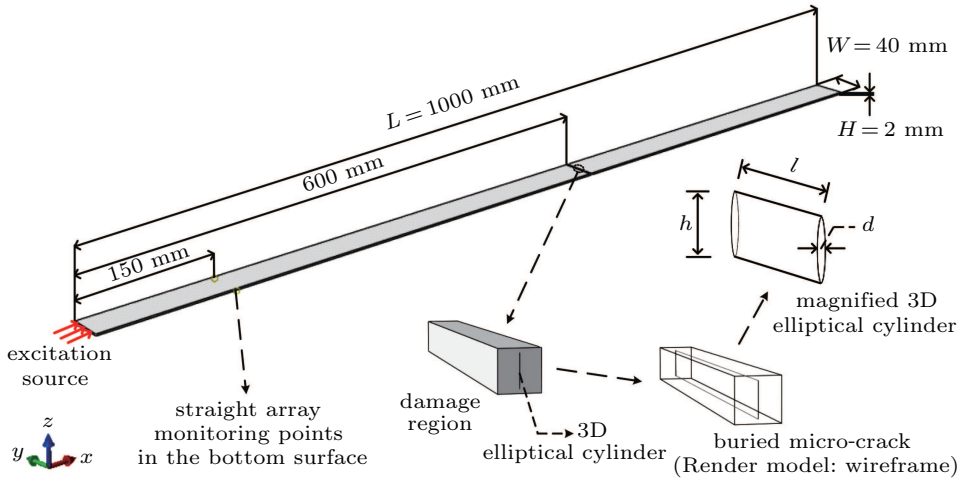


Fig. 2. Aluminum plate 3D model dimensions and damage modes.

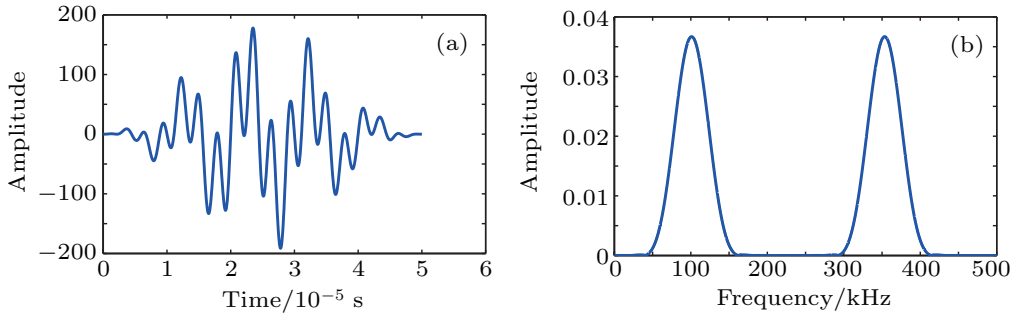


Fig. 3. Excitation signals in aluminum plate, showing (a) time domain spectrum and (b) frequency domain spectrum.

In the aluminum plate model, the buried micro-crack was located 600 mm away from the left side surface in the x direction, and was modeled as an elliptical cylinder (Fig. 2) with hard contact frictionless surface.[31] Receiving points were 150 mm away from the left side surface. Specified binding constraint was established between the long plate master and slave surface of the damage region to ensure simulation accuracy and efficiency (Fig. 2). Micro-crack damage detection was simulated by adjusting the elliptical cylinder dimensions l, h, and d (Fig. 2).

A suitable mesh division method was devised to ensure computational accuracy and model efficiency. Although

smaller mesh elements can improve computational accuracy, this also requires more calculation times and computer resources. Therefore, appropriate mesh density and computational time step should be selected for the model to ensure that the system simulation requirements are satisfied.

For 100-kHz and 350-kHz mixed signals in the aluminum plate model, following Eqs. (9) and (10),[34] appropriate mesh element size and time step were $L_{\max} = 0.6$ mm and $\Delta t_{\max} =$ 110 ns, respectively. However, we chose a finer mesh element size $L_{\max} = 0.4$ mm for the micro-crack zone to improve calculation accuracy, hence

$$L_{\max} = \frac{\lambda_{\min}}{20} = \frac{C_{\mathrm{p}}}{20 f_{\max}}, \tag{9}$$

$$\Delta t_{\max} = \frac{1}{20 f_{\max}}. \tag{10}$$

3.1.2. Composite laminate 3D models

In this study, we also simulated 3D thin composite laminates, where composite laminate model size was the same as that for the aluminum plate. Table 2 shows the T300/QY8911 composite lamina material properties.

Table 2. T300/QY8911 composite lamina material properties.

E_1/GPa	E_2/GPa	E_3/GPa	G_{12}/GPa	G_{13}/GPa	G_{23}/GPa	ν_{12}	ν_{13}	ν_{23}	ρ/(kg/m^3)
135	8.8	8.8	4.47	4.47	3.45	0.3	0.3	0.34	1560

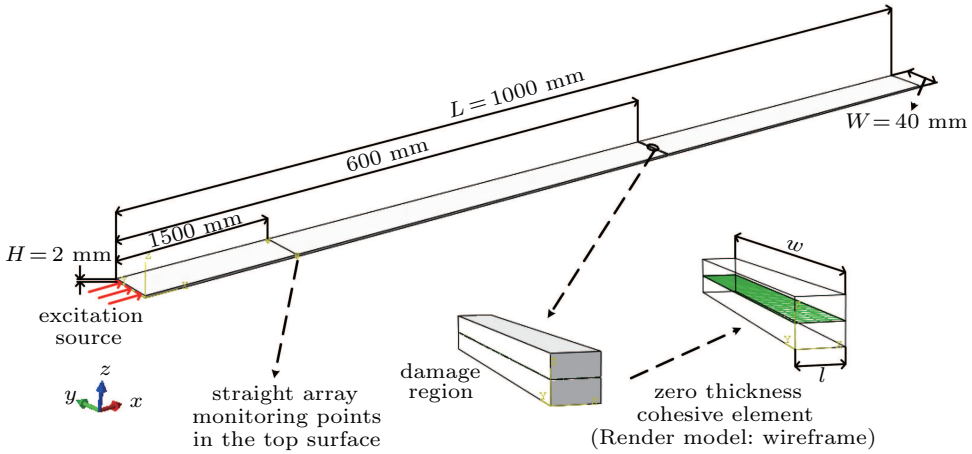


Fig. 4. Composite laminate 3D model dimensions and damage modes.

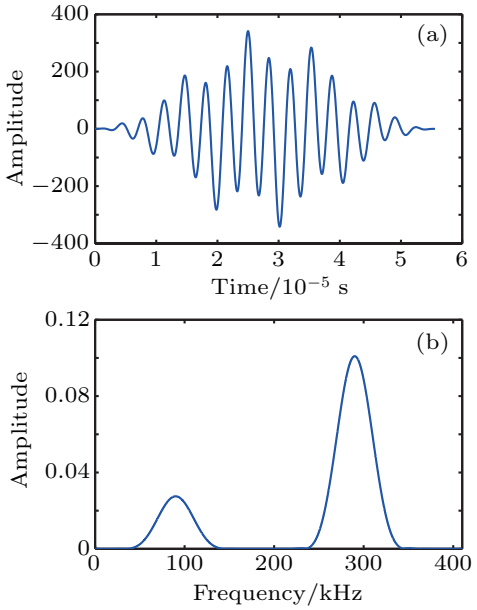


Fig. 5. Composite laminate excitation signal, showing plot of amplitude *versus* (a) time and (b) frequency.

Model size, damage region, and other parameters were generally consistent with those for the aluminum plate model (Fig. 4). The mesh element size for the whole model was calculated from Eqs. (9) and (10) and we selected an appropriate mesh size $L_{\max} = 0.5$ mm. Source signal center frequencies became 90 kHz and 290 kHz. Figure 5 shows the excitation signal and corresponding frequency domain spectrum.

Since each individual composite laminate layer was composed of the same fiber reinforced material, a local coordinate system was created to exhibit lamina material properties.[35] Ten ply layers were used to generate a quasi-isotropic layup sequence $[45/-45/0/90/45]_{\mathrm{s}}$,[36] where figure 6 shows the corresponding ply stack. Composite laminate damage type (delamination) was different from that for aluminum plate, which was placed between the fifth and sixth layers (see Fig. 4). First, composite laminate delamination damage was characterized by cohesive element damage and failure. Second, cohesive element thickness = zero,[37–39] hence duplicate nodes were numbered at the same location to simulate delamination damage. Consequently, we adjusted cohesive element dimensions (l and w with zero thickness) (Fig. 4) to simulate damage detection.

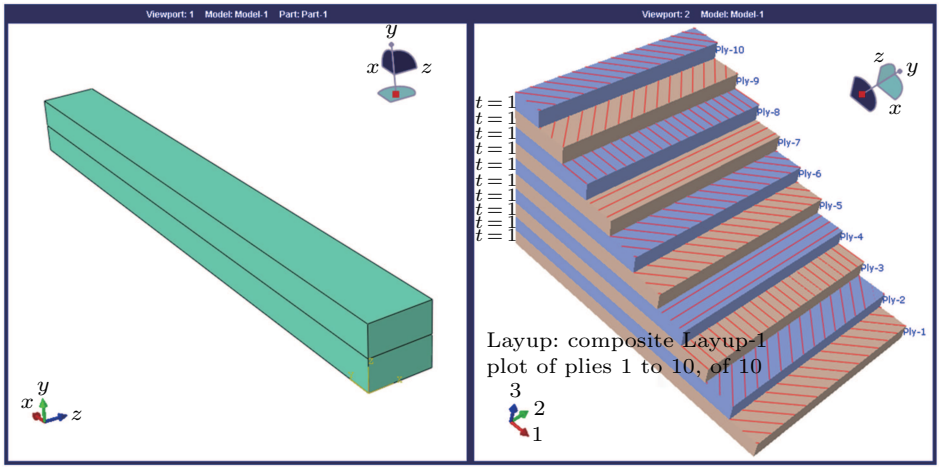


Fig. 6. Composite material ply orientation and ply number diagram of the damaged region.

3.2. Simulation results and analyses

3.2.1. Time-domain simulation results

After establishing the 3D aluminum plate model, we conduct a comparative initial time domain response analysis for undamaged and damaged plate with a buried micro-crack 20 mm×1.6 mm×0.0001 mm (length (l) × height (h) × thickness (d)) as shown in Fig. 2. Figure 7 shows that the received time domain signals indicate the interaction between the Lamb wave and micro-crack. Figure 8 shows the same operation for undamaged and damaged composite laminates with zero thickness cohesive element 2 mm×20 mm (length (l) × width (w)) (Fig. 4).

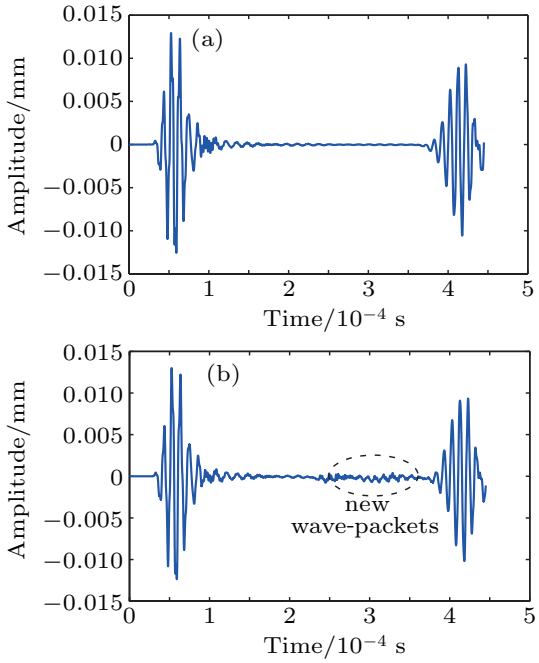


Fig. 7. Time domain signal received from 3D (a) undamaged and (b) micro-cracked aluminum plate.

Figures 7 and 8 show that the new wave packets are generated in the time domain simulation signal for the damaged plate. The first wave packets in Figs. 7(a) and 8(a) are the direct S_0 mode waves due to the excitation signal, with the other wave packets being reflected waves from the right side surface. New wave packets in Figs. 7(b) and 8(b) are S_0 mode packets produced by crack damage and mixed wave packets that include re-reflected signals from the left side surface of the S_0 mode wave produced by the crack and A_0 mode caused by nonlinear crack or damage effects, respectively.

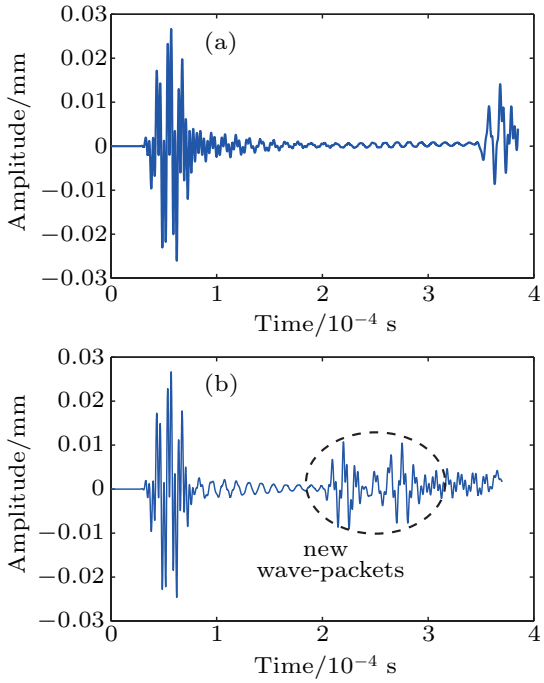


Fig. 8. Time domain signal received from 3D (a) undamaged and (b) damaged composite laminate plate.

In Fig. 9 the time domain wave packet for aluminum plate is compared with that for composite laminate, showing the obvious differences between undamaged and damaged thin plate simulations. Therefore, the nonlinear effect is embodied in new wave packets containing micro-crack or damage flaw information.

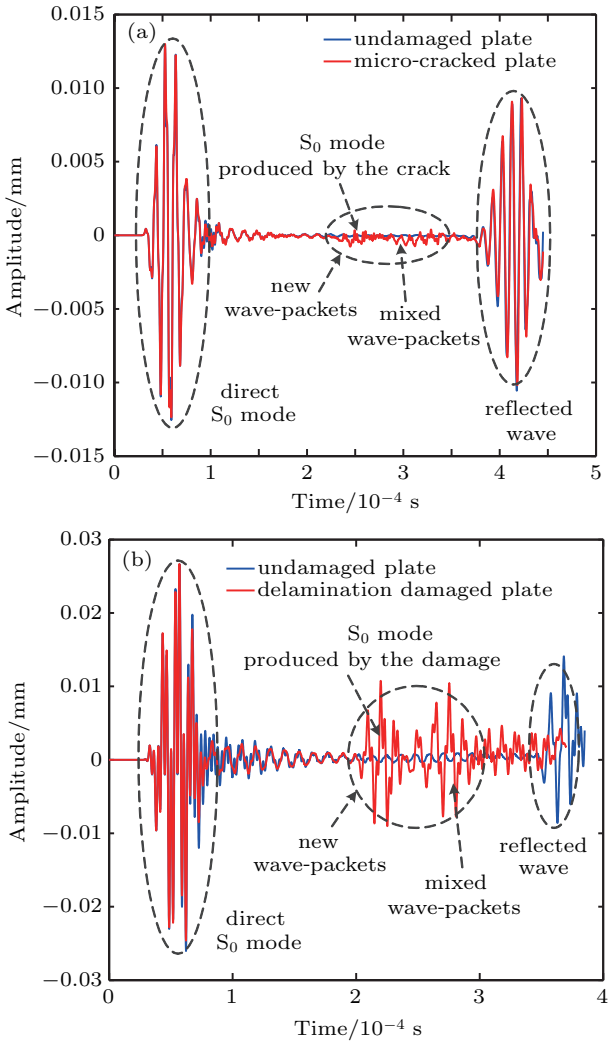


Fig. 9. Superimposed time domain signals from undamaged and damaged (a) aluminum plate and (b) composite laminate.

3.2.2. Frequency domain simulation results

More comprehensive analyses can be studied in the frequency domain. Figure 10 shows FFT of the new wave packets for undamaged and damaged aluminum plate and composite laminate.

Figure 10(a) shows that four amplitude peaks appear respectively at approximately 100, 250, 350, and 450 kHz for the micro-cracked plate, but only two peaks arise at approximately 100 kHz and 350 kHz for the undamaged plate. Since excitation signal frequencies are centered at 100 kHz and 350 kHz, the undamaged plate peaks correspond to the fundamental frequency component amplitudes, whereas the 250 kHz and 450 kHz peaks correspond to difference and sum frequency component amplitudes.

Figure 10(b) shows four peaks respectively at 90, 200, 290, and 380 kHz for the composite laminates, where 90-kHz and 290-kHz peaks correspond to fundamental frequency component amplitudes, and 200-kHz and 380-kHz peaks correspond to the difference and sum frequency component amplitudes.

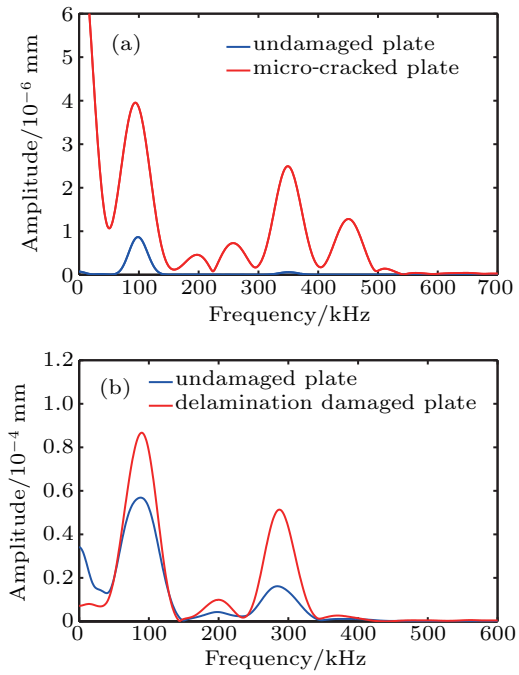


Fig. 10. Frequency-dependent spectra for (a) aluminum plate and (b) composite laminate.

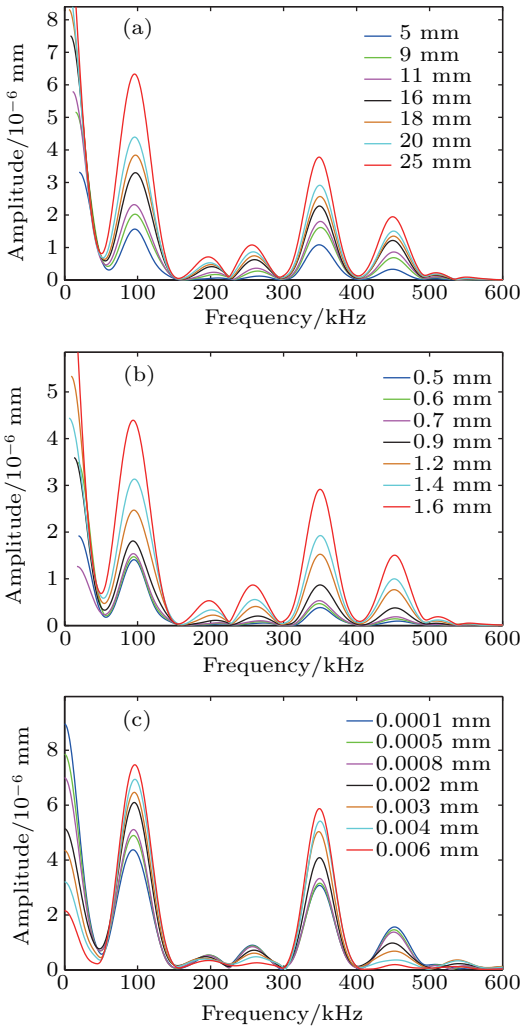


Fig. 11. Comparison among wave packet spectra from 3D aluminum plate with buried micro-cracks of various sizes under (a) equal height and thickness with different lengths, (b) equal length and thickness with different heights, and (c) equal length and height with different thickness values.

Signal amplitudes in the frequency domain for damaged plate are significantly larger than for undamaged plate (Fig. 10), implying that the new wave packet generated from micro-cracked or delamination damaged plates consist of sum and difference frequency components, and these frequency components are produced by the defects. Hence, these generated frequency components provide a sensitive tool for damage detection.

To investigate the relationship between nonlinear effects and buried micro-crack or delamination damage dimension, several simulations are performed for the 3D aluminum plate with various micro-crack sizes. Group 1 is for simulating the buried micro-cracks with fixed height and thickness ($h =$ 1.6 mm, $d = 0.0001$ mm) and various lengths ($l = 5$, 9, 11, 16, 18, 20, and 25 mm). Group 2 is for simulating the buried micro-cracks of fixed length and thickness ($l = 20$ mm and $d = 0.0001$ mm) and various heights ($h = 0.5$, 0.6, 0.7, 0.9, 1.2, 1.4, and 1.6 mm). Finally, group 3 is for simulating the buried micro-cracks with fixed length and height ($l = 20$ mm and $h = 1.6$ mm) and various thicknesses ($d = 0.0001$, 0.0005, 0.0008, 0.002, 0.003, 0.004, and 0.006 mm). The corresponding simulation results are shown in Fig. 11.

Two simulation groups are also investigated for different delamination damage dimensions in 3D composite laminates. In group 4 considered are the zero thickness cohesive elements with constant width ($w = 20$ mm) and various lengths ($l = 1.2$, 1.3, 1.5, 1.6, 1.7, and 2 mm). In group 5 considered are the zero thickness cohesive elements with constant length ($l = 2$ mm) and various widths ($w = 8$, 10, 13, 15, 17, and 20 mm). Figure 12 shows the corresponding numerical simulation results.

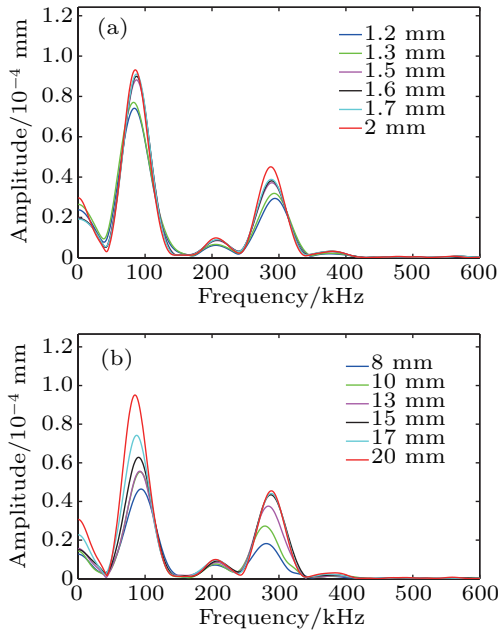


Fig. 12. Comparison among wave-packet spectra from 3D composite laminates with zero thickness cohesive elements under (a) equal width with different lengths and (b) equal length with different widths.

Figure 11 shows that fundamental frequency signal (100 kHz and 350 kHz) amplitudes have significant positive correlation with buried micro-crack length, height, and thickness for the aluminum plates. Sum and difference frequency (450 kHz and 250 kHz, respectively) signal amplitudes positively relate to micro-crack length and height, and negatively relate to micro-crack thickness. Figure 12 shows that fundamental (90 kHz and 290 kHz), sum (380 kHz), and difference (200 kHz) frequency amplitudes all have significant positive correlation with length and width of the zero thickness cohesive element. These indicate that sum and the difference frequency amplitudes have significant dependence on micro-crack size and zero thickness cohesive element. Therefore, nonlinear sources in the structure, such as micro-cracks or delamination damage, can be determined based on sum and difference frequency components in frequency domain nonlinear response.

3.2.3. Amplitude ratio results

We investigate the change rule for nonlinear signals. From the observed signal amplitudes, we analyzed β, (Eq. (8)), define β_1 and β_2 as[22]

$$\beta_1 = \frac{A_3}{A_1 A_2}, \tag{11}$$

$$\beta_2 = \frac{A_4}{A_1 A_2}, \tag{12}$$

where A_3 and A_4 represent the sum and difference frequency signal amplitudes, respectively, β_1 expresses the amplitude ratio for the sum frequency component, and β_2 for the difference frequency component. Figure 13 shows the derived amplitude ratios for the aluminum plate.

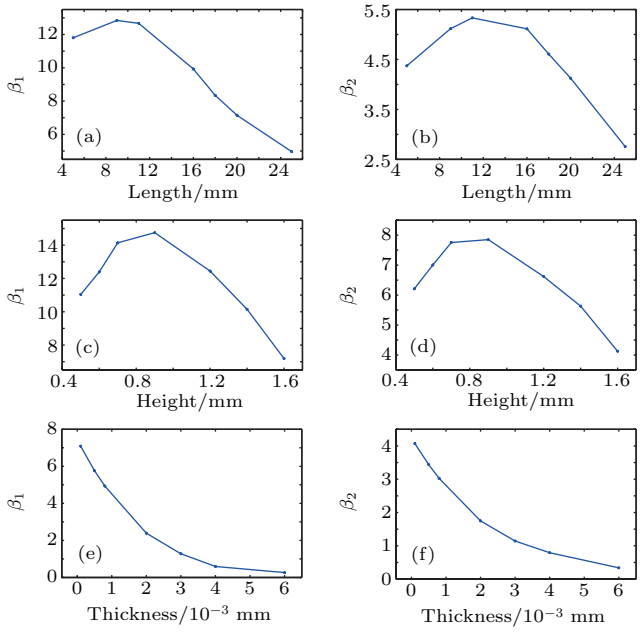


Fig. 13. Amplitude ratio (β_1 and β_2) variations for different ((a), (b)) micro-cracks (c) lengths, (d) heights, and ((e), (f)) thickness values in aluminum plate.

Figure 13 shows that β_1 and β_2 first increase and then decrease with the increase of micro-crack length and height in the aluminum plate, whereas they monotonically decrease with micro-crack thickness increasing. Micro-crack area increases as the micro-crack becomes longer and higher, hence enlarging the contact surface between the Lamb wave and crack (see Figs. 11(a) and 11(b)). Therefore, incident waves mostly encounter the crack and then propagate to the left side surface after reflection. Consequently, A_1, A_2, A_3, and A_4 increase, but growth of A_1 and A_2 exceed faster that of A_3 and A_4, hence β_1 and β_2 reach a peak and then fall down to relatively low levels (Figs. 13(a) and 13(b), Figs. 13(c) and 13(b)) with crack area increasing. Figure 11(c) show that A_1 and A_2 increase as thickness increases, whereas A_3 and A_4 reduce gradually. Consequently, corresponding β_1 and β_2 decrease monotonically (Figs. 13(e) and 13(f)).

Thus, amplitude ratios strongly depend on micro-crack dimensions, *i.e.*, acoustic nonlinearity decreases as the 3D buried micro-crack thickens. Consequently, the nonlinear Lamb wave S_0 mode exhibits greater sensitivity to buried micro-crack thickness in thin 3D aluminum plate.

Amplitude ratio variations for composite laminates exhibit different trends (Fig. 14). Figures 12(a) and 12(b) show that damage areas, A_1, A_2, A_3, and A_4 increase as delamination damage (zero thickness cohesive element) becomes longer and wider. Figures 14(a) and 14(b) show different tendencies for amplitude ratio variation with cohesive element length increasing: β_1 increases and then decreases, whereas β_2 decreases monotonically. Figures 14(c) and 14(d) show that sum and difference frequency amplitude ratio decreases with wider cohesive element increasing. Therefore, the nonlinear Lamb wave exhibits greater sensitivity to buried zero thickness cohesive element width for 3D thin composite laminate.

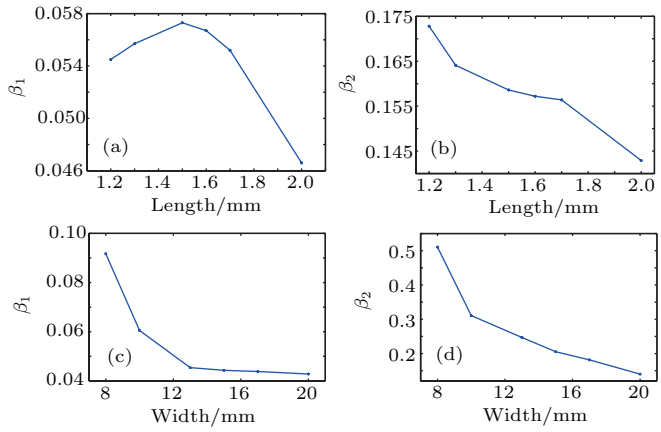


Fig. 14. Amplitude ratio (β_1 and β_2) variations for different (a) micro-cracks, (b) lengths, and ((c), (d)) width of zero thickness cohesive element in composite laminates.

The proposed method relies only on the Fourier spectrum amplitude ratio rather than any other baseline data. Thus, the amplitude ratio acts as indicator to identify incipient buried micro-crack or delamination damage. This has potential applications in internal defect detection in thin plates through using nonlinear Lamb waves.

4. Conclusions

We construct 3D finite element numerical model for thin aluminum plate with buried micro-cracks and that for composite laminates with inner delamination damage to investigate Lamb wave nonlinear phenomena for mixed-frequency excitation. Some conclusions are drawn as follows.

(i) Time domain simulations of undamaged and damaged plates show that new wave packets appear due to the interaction between the nonlinear Lamb wave and micro-crack or delamination damage. Thus, the new wave packets are the main research objects.

(ii) Frequency domain analyses of wave-packet FFT for undamaged and damaged plate aluminum plate and composite laminate are performed. The FFT is mainly applied to the new wave packets in the damaged plates. Simulation results confirm the existence of sum and difference frequencies components. The sum and difference frequency amplitude variations are analyzed respectively by changing micro-crack length (l), height (h), thickness (d), delamination damage length (l), and width (w). Different sizes exhibit different nonlinear behaviors, confirming that the sum and difference frequencies provide a sensitive tool for defect detection.

(iii) The sum and difference frequency amplitude ratio variations are investigated and shown to be strongly dependent on micro-crack or delamination damage dimensions. Combined with the nonlinear Lamb wave variation sensitivity to different defects size parameters, the unique amplitude ratio can provide an important index for defect detection.

Thus, the simulation results of aluminum plate and composite laminate provide a feasible method to identify and evaluate the incipient crack defects in thin 3D plate structures with mixed nonlinear Lamb waves. Also, the research in this paper will provide theoretical guidance for future laboratory research.

References

[1] Yang R Z, He Y Z and Zhang H 2016 *Renew. Sust. Energ. Rev.* **60** 1225
[2] Mańka M, Rosiek M, Martowicz A, Stepinski T and Uhl T 2016 *Mech. Syst. Sig. Process.* **78** 71
[3] Shan S B, Cheng L and Li P 2017 *Smart Mater. Struct.* **26** 025019
[4] Cawley P and Alleyne D 1996 *Ultrasonics* **34** 287
[5] Gao H and Rose J L 2010 *Aeronaut. J.* **114** 49
[6] Jhang K Y 2009 *Int. J. Precis. Eng. Man.* **10** 123
[7] Broda D, Staszewski W J, Martowicz A, Uhl T and Silberschmidt V V 2014 *J. Sound Vib.* **333** 1097
[8] Chen J, Xu Z, Yu Y and Yao Y P 2014 *NDT E Int.* **67** 10
[9] Delrue S and Koen V D A 2015 *Ultrasonics* **63** 147
[10] Novak A, Bentahar M, Tournat V, Guerjouma R E and Simon L 2012 *NDT E Int.* **45** 1
[11] Wan X, Tse P W, Chen J M, Xu G H and Zhang Q 2018 *Ultrasonics* **82** 57

[12] Jiao J P, Sun J, Li N, Song G R, Wu B and He C F 2014 *NDT E Int.* **62** 122
[13] Zhou J Y, Xiao L, Qu W Z and Lu Y 2017 *NDT E Int.* **92** 22
[14] Antonaci P, Bruno C L E, Bocca P G, Scalerandi M and Gliozzi A S 2010 *Cem. Concr. Res.* **40** 340
[15] Kudela P, Radzienski M, Ostachowicz W and Yang Z B 2018 *Mech. Syst. Signal Process.* **108** 21
[16] Wan X, Tse P W, Xu G H, Tao T F and Zhang Q 2016 *Smart Mater. Struct.* **25** 045023
[17] Wang Y, Guan R and Lu Y 2017 *Ultrasonics* **80** 87
[18] Zhao Y X, Li F L, Cao P, Liu Y L, Zhang J Y and Fu S Y 2017 *Ultrasonics* **79** 60
[19] Sotoudeh V, Black R J, Moslehi B and Qiao P Z 2014 *Proc. SPIE* **9062** 2978
[20] Yang Y, Ng C T and Kotousov A 2018 *Smart Mater. Struct.* **27** 055013
[21] Li W B, Cho Y and Achenbach J D 2012 *Smart Mater. Struct.* **21** 085019
[22] Jiao J P, Meng X J, He C F and Wu B 2017 *NDT E Int.* **85** 63
[23] Li F L, Zhao Y X, Cao P and Hu N 2018 *Ultrasonics* **87** 33
[24] Sun M X, Xiang Y X, Deng M X, Xu J C and Xuan F Z 2018 *NDT E Int.* **93** 1
[25] Lee D J, Cho Y and Li W B 2014 *AIP Conf. Proc.* **1581** 662
[26] Pai P F, Deng H G and Sundaresan M J 2015 *Mech. Syst. Sig. Process.* **62–63** 183
[27] Shen Y F and Giurgiutiu V 2015 *Wave Motion* **58** 22
[28] Rauter N, Lammering R and Kühnrich T 2016 *Compos. Struct.* **152** 247
[29] Ben B S, Ben B A, Vikram K A and Yang S H 2013 *Measurement* **46** 904
[30] Ochôa P, Infante V, Silva J M and Groves R M 2015 *Compos. Part. B-Eng.* **80** 291
[31] Wan X, Zhang Q, Xu G H and Tse P W 2014 *Sensors* **14** 8528
[32] Yelve N P, Mitra M and Mujumdar P M 2013 *Struct. Control. Hlth.* **21** 833
[33] Jiao J P, Sun J J, Li G H, Wu B and He C F 2015 *NDT E Int.* **69** 1
[34] Shen Y F and Giurgiutiu V 2014 *J. Intel. Mat. Syst. Str.* **25** 506
[35] He C F, Liu H Y, Liu Z H and Wu B 2013 *J. Sound Vib.* **332** 7243
[36] Sherafat M H, Quaegebeur N, Hubert P, Lessard L and Masson P 2016 *J. Reinf. Plast. Comp.* **35** 796
[37] Sarrado C, Leone F S and Turno A 2016 *Eng. Fract. Mech.* **168** 105
[38] Jiang H X and Meng D G 2018 *Eng. Fract. Mech.* **199** 280
[39] Carreras L, Bak B L V, Turon A, Renart J and Lindgaard E 2018 *Eur. J. Mech. A-Solid* **72** 464